Bulletin of the Seismological Society of America, Vol. 86, No. 3, pp. 797–804, June 1996

Source Estimation of Finite Faults from Broadband Regional Networks

by Xi J. Song and Donald V. Helmberger

Abstract Fast estimation of point-source parameters for earthquakes has progressed much in recent years due to the development of broadband seismic networks. The expansion of these networks now provides the opportunity to investigate second-order effects such as source finiteness for regional and local events on a routine basis. This potential motivates the development of methods to quickly generate synthetic seismograms for finite sources. This is possible when the fault dimension is small compared to the source-receiver distance and when the structure around the source region is relatively simple. To study the directivity for a finite source, we discretize the fault region into a set of elements represented as point sources. We then generate the generalized rays for the best-fitting point-source location and derive for each separate ray the response for neighboring point sources using power series expansions. The response for a finite fault is then a summation over rays and elements. If we sum over elements first, we obtain an effective far-field source-time function for each ray, which is sensitive to the direction of rupture. These far-field source-time functions are convolved with the corresponding rays, and the results are summed to form the total response. A simple application of the above method is demonstrated with the tangential motions observed from the 1991 Sierra Madre earthquake. For this event, we constrain the fault dimension to be about 3 km with rupture toward the west, which is compatible with other more detailed studies.

Introduction

In recent years, due to the development of broadband seismic networks, the estimation of point-source parameters for earthquakes using regional records has been made faster and more reliable (e.g., Thio and Kanamori, 1995; Ritsema and Lay, 1995; Walter, 1993; Dreger and Helmberger, 1991; Patton and Zandt, 1991). Zhao and Helmberger (1994) developed a grid-search method to estimate point-source orientation, depth, magnitude, and duration with broadband data. Scrivner and Helmberger (1994) recently utilized this technique in their preliminary work on developing an early warning system. However, synthetic fits to waveform data for many earthquakes could be significantly improved by adding directivity or fault finiteness, which indicates that source finiteness plays an important role for many moderate to large earthquakes. Thus, being able to quickly estimate such characteristics and generate synthetics for complex sources would be highly useful. Current methods used for generating responses from complex sources rely on direct summation of point-source responses or approximate reflectivity approaches based on source decomposition (Saikia and Helmberger, 1996), which are both time-consuming processes. Here, we introduce a method based on the generalized ray theory (Helmberger, 1983) to efficiently compute synthetic seismograms for complex sources. This technique can be applied to faults with small dimensions compared to the source-receiver distance, in regions where the structure around the source can be modeled as a layer of constant velocity. We apply this method to estimate the source dimension and general directivity of the 1991 Sierra Madre, California, earthquake. This event occurred in the middle of the TERRAscope array (Fig. 1) and was well studied (e.g., Dreger and Helmberger, 1991; Wald, 1992). The latter study used a large collection of local data, strong-motion, and teleseismic seismograms to establish rupturing to the southwest. Comparing our results against this solution illustrates the usefulness of our new technique.

Method

From the generalized ray theory (Helmberger, 1983), for a layered half-space, a generalized ray with ray parameter p_0 is associated with the characteristic travel time, t_0,

$$t_0 = p_0 r + \sum_i \eta_i d_i, \tag{1}$$

where r is the source-receiver distance, η_i is the vertical slowness of the ray in each layer, and d_i is the vertical distance of the ray segment in each layer. If the paths from two point sources are close, the responses at the receiver for the

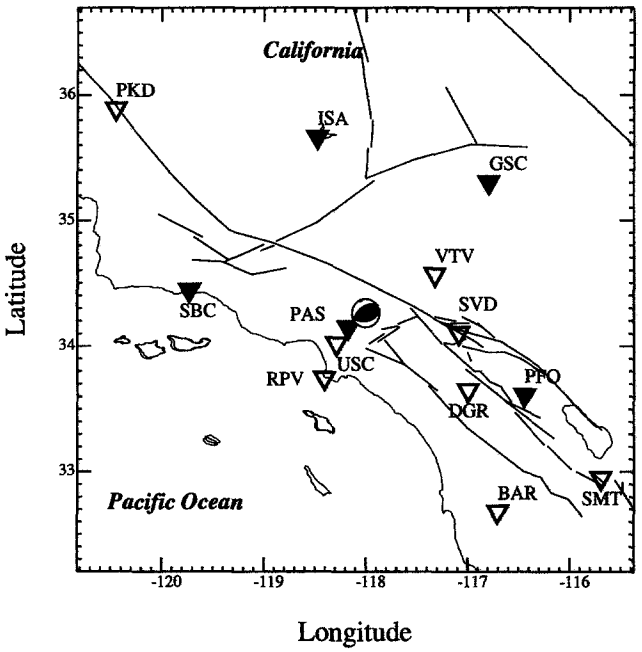

Figure 1. Broadband stations (triangles) located in southern California. Stations used in this study are plotted as solid triangles. The source mechanism of the Sierra Madre earthquake, determined by Dreger and Helmberger (1992), is shown at the epicenter.

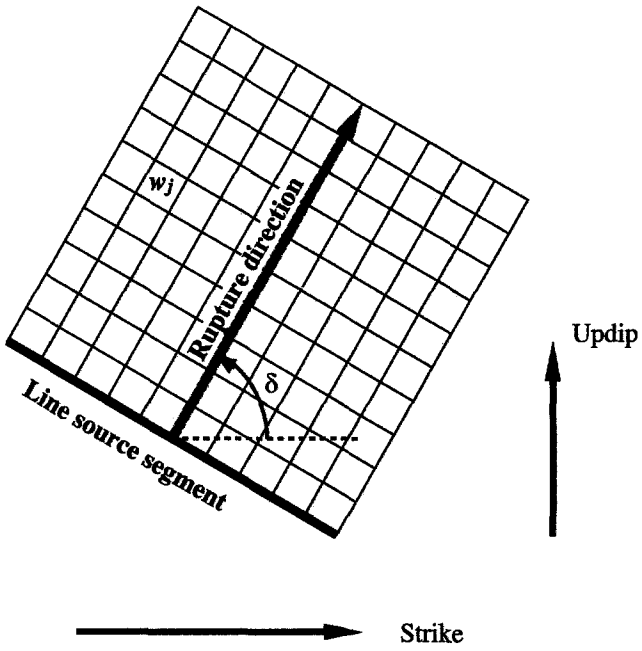

Figure 2. Map view of a discretized fault. Rupture is simulated by a line source segment propagating perpendicular to itself. The rupture angle δ, relative to the fault strike, is defined here to specify the rupture direction. When calculating the synthetic seismograms, each element of the fault is represented by a point source with a weighting factor $w_j \cdot w_j = 1$ is used in this study.

two point sources are similar in shape and amplitude and differ primarily by a small time shift, dt_0 (Helmberger *et al.*, 1992). As an approximation, we treat p_0 as constant and use a Taylor-series expansion for t_0 around the point-source position (r, h) to represent the time variance dt_0. That is,

$$dt_0 = \frac{\partial t_0}{\partial r} dr + \frac{\partial t_0}{\partial h} dh \tag{2}$$

with $\partial t_0/\partial r = p_0$ and $\partial t_0/\partial h = -\varepsilon\eta_s$, where $\varepsilon = 1$ for down-going rays and $\varepsilon = -1$ for up-going rays. $\eta_s = [(1/v_s^2) - p_0^2]^{1/2}$ is the vertical slowness of the ray p_0 in the source region, and v_s is the velocity in the source region. For a finite fault, we discretize the rupture region into a set of elements, each represented as a point source (Fig. 2). The total response, $s_j(t)$, at the receiver for a point-source j in the neighborhood of the reference point source can be derived from that for the reference point source by summing the rays, each properly lagged in time.

$$s_j(t) = \left[\sum_i R_i(t - dt_{0ij})\right] * f(t). \tag{3}$$

$R_i(t)$ is the response for ray i for the reference point source, and Σ_i indicates summation over rays. If the point source is not a step dislocation, a far-field source-time function $f(t)$ is used, as in equation (3). Equation (3) is justified if we avoid source radiation nodes by omitting nodal stations.

To illustrate that the Taylor-series expansion and the shift technique are reasonable approximations, we compared the point-source responses that are calculated with equation (3) for the standard Southern California model (SC, Table 1) and those calculated exactly (Fig. 3). Some of the more important ray responses for a source at a depth of 12 km are displayed in Figure 4. As the source changes depth, these arrivals interfere with each other, with the Love wave showing the most variation, as displayed in Figure 3. The similarity of these two sets of responses demonstrates that the timing of the individual rays is a more important parameter than the change in individual wave shape.

For the finite fault, a time lag dT_j is applied to each point source to simulate the propagation of the rupture front across the fault, and the total response $S(t)$ at the receiver is the sum of those for all the point sources,

$$\begin{aligned} S(t) &= \sum_j w_j s_j(t - dT_j) \\ &= \sum_j w_j \left[\sum_i R_i(t - dt_{0ij} - dT_j)\right] * f(t), \end{aligned} \tag{4}$$

where Σ_j indicates summation over point sources and w_j is the weighting factor for point-source j, representing slip distribution on the fault plane (Fig. 2). If we generate and store the separate generalized rays for the best-fitting point-source

Table 1
Model Parameters (After Dreger and Helmberger, 1991)

Model LOHS1				Model SC			
V_p (km/sec)	V_s (km/sec)	ρ (g/cc)	Z^* (km)	V_p (km/sec)	V_s (km/sec)	ρ (g/cc)	Z (km)
4.5	2.6	2.4	0.0	5.5	3.18	2.4	0.0
5.9	3.5	2.67	4.0	6.3	3.64	2.67	5.5
6.6	3.8	2.8	16.0	6.7	3.87	2.8	16.0
8.0	4.1	3.1	26.0	7.8	4.5	3.0	35.0
8.2	4.2	3.3	30.0				

*Z is the depth to the top of the layer.

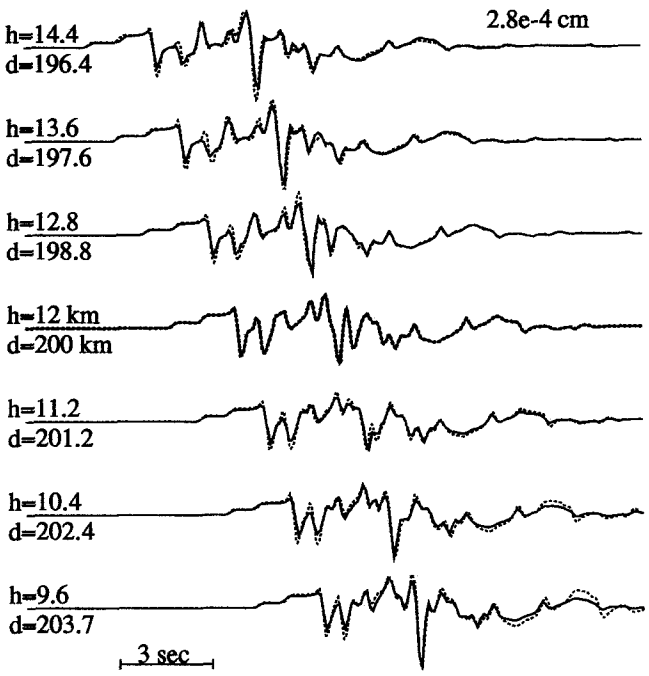

Figure 3. A set of point sources is used to simulate a linear rupture on a fault plane (strike 242°, dip 50°, rake 74°). Rupture starts at a depth of 14.4 km with a rupture angle 45°. Seven point sources on this line are selected here for comparison. Each dashed trace is the point-source response in displacement at the receiver for the given distance and depth. These point-source responses are calculated independently and shifted properly to reflect the origin-time difference due to rupture, as in a conventional point-source summation procedure. Solid traces are point-source responses at the same receivers derived from the response for the $h = 12$ km point source by lagging each ray properly to reflect the origin-time difference due to rupture and the travel-time difference due to varying point-source positions using the Taylor-series expansion approximation for t_0. Crustal model SC (Table 1) is used for the calculations, and a far-field source-time function (0.2, 0.2 sec) is used for each point source. Seismograms are plotted on the same scale with the amplitude of the first solid trace shown.

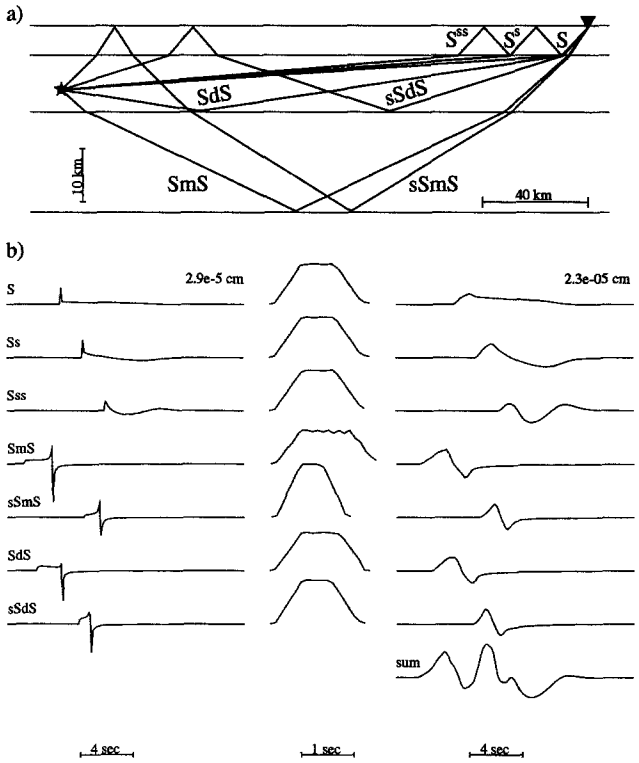

Figure 4. (a) Paths of some of the important rays shown in (b). The star indicates the source, and the triangle, the receiver. (b) Ray responses (left column, displacement) and the corresponding unit-area far-field source-time functions (middle column, with a different time scale). Each ray is convolved with its corresponding far-field source-time function, and the results (right column) are summed to form the total response (the right bottom trace) from the complex source. In this example, a 3-km-long line source segment propagates 2 km up-dip from a depth of 12 km at a constant velocity 3.0 km/sec on a fault plane striking 242° and dipping 50°. Source-receiver distance is 200 km, and the station azimuth is 44°. Seismograms are plotted on the same scale with the amplitude of the first trace in each column shown. A far-field source-time function (0.1, 0.1, 0.1 sec) is used for each point source. Model SC (Table 1) is used.

location, we can then shift each ray accordingly and sum them to form the total response of a complex source, as in equation (4).

Rearranging the summation, equation (4) can be rewritten as

$$S(t) = \sum_j w_j \left[\sum_i R_i(t) * \delta(t - dt_{0_{ij}} - dT_j) \right] * f(t) = \sum_i R_i(t) * \sum_j w_j [\delta(t - dt_{0_{ij}} - dT_j) * f(t)]. \quad (5)$$

In this manner, we have defined a far-field source-time function

$$F_i(t) = f(t) * \sum_j w_j \delta(t - dt_{0_{ij}} - dT_j) \quad (6)$$

for ray i as the result of the rupture across the finite fault. Equation (6) is similar to equation (A1) in Langston (1978), except that the latter approximates $dt_{0_{ij}}$ with an analytic expression that is appropriate for teleseismic rays. From this point of view, the total response at the receiver can be seen as the summation of all the generalized rays convolved with corresponding far-field source-time functions.

In Figure 4b, a set of rays are selected to demonstrate the process of building the total response for a complex source via equation (5). Note that each ray, unlike rays from a point source, has its own individual source-time function dependent on its ray parameter. In this case of up-going rupture, the source-time functions for down-going rays (e.g., *SmS*, *SdS*) have longer durations than those for up-going rays (e.g., *sSmS*, *sSdS*). Given the fault geometry and the faulting characteristics, one can generate synthetics in this way much faster than direct summation of point-source responses. In the next section, we will apply this technique to a forward-search procedure to constrain the fault dimension and directivity.

Application

The simplest application of the above method is to estimate the source dimension and general directivity of an earthquake assuming models with no asperities. We applied our method to the 1991 Sierra Madre earthquake, which occurred in the middle of the TERRAscope array and was well recorded at stations PFO, GSC, ISA, and SBC. Although we did not restrict the response $S(t)$ in equation (5) to be the tangential motion, we will use only the tangential components in this experiment to reduce the number of rays involved for simplicity. We use the tangential components of broadband data from the four stations PFO, GSC, ISA, and SBC to estimate the fault dimension and the rupture direction. Broadband records of this event were inverted by Dreger and Helmberger (1991) to obtain a point-source solution with strike 235°, dip 50°, and rake 74°. They used a triangular far-field source-time function with a duration of 1 sec, determined by measuring the width of the tangential component direct *S*-wave recorded at station PAS.

We investigate the fault dimension and general directivity via a forward-search approach, using simple fault models of square faults with uniform slip. Using the Haskell model (Haskell, 1964), a finite fault is simulated with a propagating line source with a constant velocity (Fig. 2). For this earthquake, a triangular far-field slip function of duration 0.1 sec is used for the line source. We test faults of a range of dimensions. For each fault, the rupture angle is allowed to vary from 0° to 360° in increments of 15°. Synthetic seismograms are generated for each station and compared to the data. The fitness of a certain source geometry, the fault dimension and the rupture direction, is judged based on the least-squares error between data and synthetics, defined as

$$\text{Misfit} = \frac{\sum_s \left(\frac{r_s}{r_0}\right)^p \int_t [\text{Obs}(t) - \text{Syn}(t)]^2 \, dt}{\sum_s \left(\frac{r_s}{r_0}\right)^p \int_t \text{Obs}(t)^2 \, dt}, \quad (7)$$

where Σ_s indicates summation over stations. Distance correction $(r_s/r_0)^p$ is applied to give stations at different distance, r_s, approximately the same weighting (Zhu and Helmberger, 1995). r_0 = 200 km is a reference distance, and p = 1 is used in these tests since we are mostly dealing with Love waves.

Figure 5 shows the misfit between data and synthetics as a function of rupture angle on the fault plane (strike 235°, solid circles) for selected fault sizes. Although the fault size varies significantly, these functions show similar patterns, and the indicated rupture direction is not strongly related to the fault size. For this test, the functions all have smaller values for rupture angles around 270°, which indicates rupture downdip on the fault plane. The minimum misfit value for different fault sizes are at the same level, but the misfit function is more sensitive to the rupture direction for larger faults. If rupture is placed on the conjugate plane (strike 79°, open circles), smaller misfit values occur at the rupture angles around 100°, which indicates rupture updip on the conjugate plane. In both cases, the horizontal component of the rupture is toward the northwest. Figure 6 shows the comparison between data and the best-fitting synthetics for these preferred fault orientations. Synthetics for Dreger and Helmberger's (1991) point source are also shown for comparison. These synthetics fit the data in shape reasonably well, but the amplitude variation is relatively large (about 40%). In this respect, finite faults make better predictions than does the point source. In wave shape, synthetics for fault size 3 × 3 and 5 × 5 km^2 also fit the data better than the point-source synthetics, especially for stations GSC and PFO. Nevertheless, based on these misfit functions displayed in Figure 5, it is difficult to determine the fault dimension without other data. However, other finite-source inversion studies usually assume additional constraints such as moment,

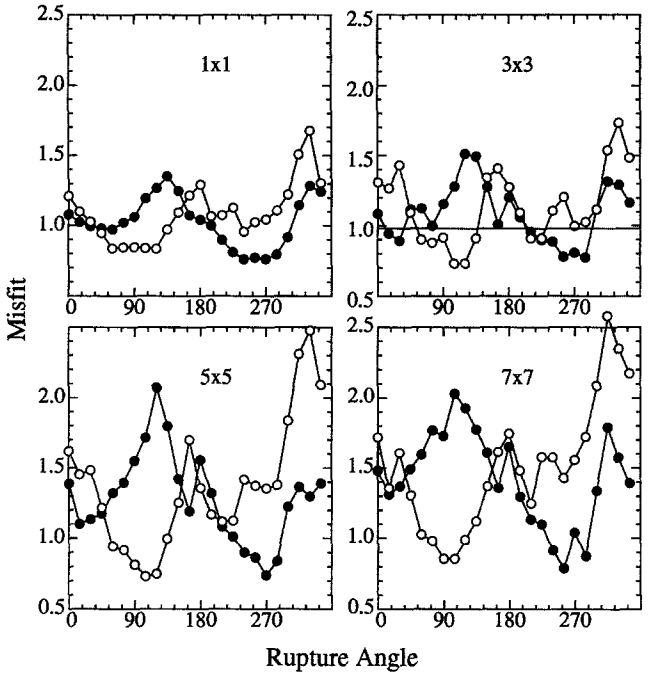

Figure 5. Misfit between data and synthetics as a function of rupture angle on the fault plane for different fault dimensions selected to model the 1991 Sierra Madre event. Solid circles are for rupture on the fault plane, and open circles, the conjugate plane. Rupture velocity is 3.1 km/sec. Stations GSC, PFO, SBC, and ISA are used, and the crustal model is SC (Table 1). The straight line in the 3 × 3 box indicates the misfit value for synthetics with Dreger and Helmberger's (1991) point source.

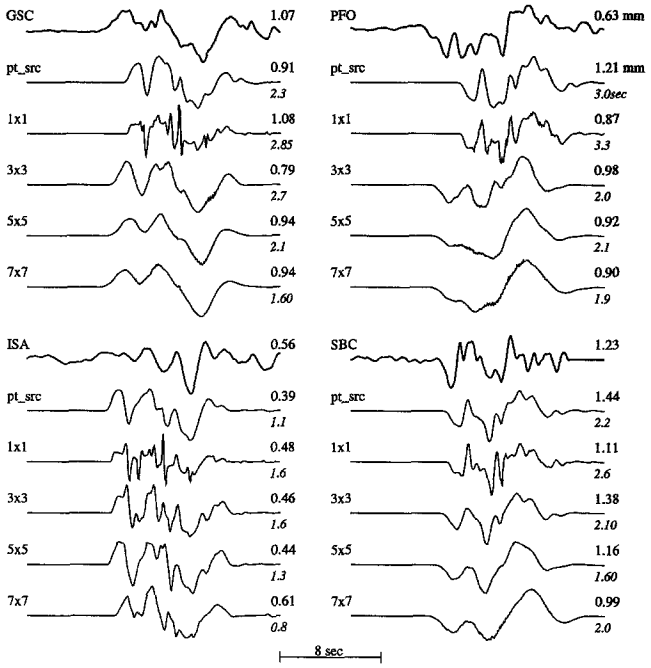

Figure 6. Comparison between data and the best-fitting synthetics for different fault sizes, for the 1991 Sierra Madre event. Fault sizes are shown at the beginning of each synthetic trace. "Pt_src" indicates Dreger and Helmberger's (1991) point source. The rupture angles used are the best ones found in the appropriate boxes in Figure 5. Synthetics are shifted in time relative to the data before computing the misfit, and the amount of shift is shown in seconds. A positive number indicates synthetic shifting to the right. Seismic moments of 3.6, 2.0, 3.6, 4.6, and 5.6 × 10^{17} N · m are used for the synthetics, respectively, as determined in the modeling process. Seismogram amplitudes are given in millimeters.

which is determined by teleseismic modeling or long-period regional inversions (Wald, 1992). If we adopt Zhao and Helmberger's (1994) moment estimates of (3.0 ± 0.7) × 10^{17} N · m, we can eliminate those fault dimensions greater than 5 km by assuming rupture velocities less than the shear velocity in the fault region. Smaller dimensions are still possible if we allow longer rise times for the line source, but a fault dimension of 3 km appears the most appropriate.

As mentioned earlier, the Taylor-series expansion and time domain shift technique in our method is most appropriate for large source-receiver distance. For short distances, the ray parameter of a generalized ray from a point source to the receiver is subject to substantial change as the position of the point source changes on the finite fault. In Figure 7, we compare the synthetics calculated via our approximation and those calculated by directly summing point-source responses for a small source-receiver distance. In each group, the seismograms are aligned in absolute timing. The comparison indicates that the approximation yields a slight shift, delay in this case, of the main energy group. The overall wave shapes are simulated reasonably well, but some high-frequency energy is lost due to the smoothing effect associated with the approximation, especially when the rupture is toward the station (Figs. 7a through 7c).

However, since we are always using imperfect Green's functions in various modeling practice, the above inadequacy does not necessarily make the approximation unusable. In cases where the major concern is the wave shape, instead of timing or amplitude, as in the procedure described above, our rough approximation provides a fast means to calculate synthetics for complex sources. This encourages us to use local stations in the procedure to constrain the fault size and general rupture direction. In this test, we use crustal model LOHS1 (Dreger and Helmberger, 1991) and the tangential motion observed at station PAS. For illustration, the synthetics for fault size 5 × 5 km^2 and varying rupture angles are compared with the data in Figure 8. Since the direct arrival (*S*) is by far the strongest pulse in the synthetics for local stations, unlike regional records, the various synthetics in Figure 8 are essentially different fits of direct *S* to the first pulse in the data. With the simple source model we are using, the far-field source-time function for direct *S* is a trapezoid, and the search among different fault sizes and rupture directions is mainly a procedure to find a trapezoid with appropriate width. When the fault size is fixed at 5 × 5 km^2,

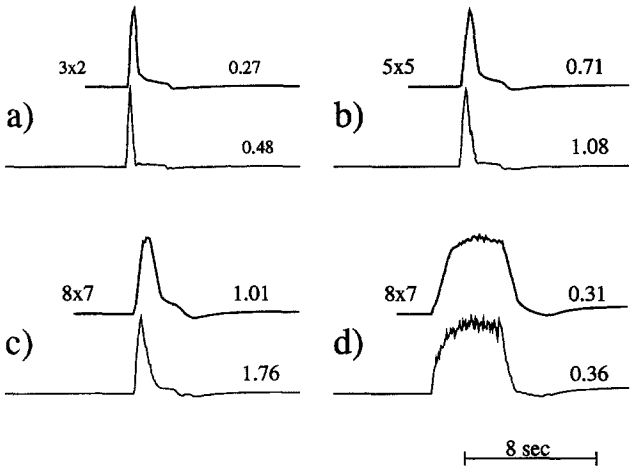

Figure 7. Comparison between synthetics calculated with our method (upper traces) and those calculated by directly summing point-source responses (lower traces) for a short distance (21 km). Fault sizes are given in kilometers. Point-source orientation is strike 235°, dip 50°, and rake 74°. Station azimuth is 232°. Rupture angles are 45° for (a), (b) and (c) and 225° for (d). Numbers at the end of each trace indicate relative peak amplitude.

rupture angles around 0° (rupture toward the southwest) are preferred. At about 200° (rupture away from PAS), the code actually fits the direct S to the first two pulses in the data. Note that there is serious trade-off between the fault size and rupture angle in affecting the width of the source-time function of one ray. This is clearly seen in Figure 9, where the misfit between synthetics and data is shown as a function of the rupture angle. When the fault size gets smaller, the pulse width, thus the misfit function, becomes less sensitive to the rupture direction. The fault with a dimension of 1 km behaves like a point source, although we do see that, on this small fault, rupture toward PAS makes the direct S pulse in the synthetics too sharp, and rupture away from PAS makes it too broad. The preferred rupture direction is actually updip or downdip. This trade-off between the fault size and the rupture direction can be avoided if better local-station coverage is provided, or we can use the information we gain from the modeling of the regional records to constrain the fault size, as discussed above. With the fault size so constrained, local data are a better indicator of the rupture direction, since it is dominated by fewer rays.

In our next experiment, we combine the local data (station PAS) with regional data (stations GSC and PFO) in the modeling process. Stations ISA and SBC were excluded since the problem with the Green's functions for these two stations are more severe than for the others (Helmberger *et al.*, 1992). The misfit functions for different fault sizes are shown in Figure 10. Figure 11 displays the fits for the preferred orientations. With these three stations, the misfit function is more sensitive to the fault size than in the previous experiments, and a fault size of 3 km is preferred based on the misfit functions. The general trend of these functions looks more or less like that in Figure 9 for station PAS only, even though we have applied the distance correction in the definition of the misfit function. This indicates that, for a given fault size, station PAS plays a dominant role in determining the general rupture direction, roughly westward in this case. In the neighborhood of this direction, the effects of the regional records become important.

Discussion and Summary

In the study of finite faults, many parameters are involved. In the above tests, we used simple square faults with fault orientation and rupture velocity fixed. Slip on the fault was also assumed to be uniform. In reality, one can either rely on other types of data to constrain parameters, such as fault orientation, total seismic moment, and rupture velocity, or one can develop more sophisticated inversion schemes to invert for these parameters together with the slip distribution. Considerable effort on the study of slip asperity has been made in the last decade (e.g., Hartzell and Heaton, 1983; Wald, 1992). With the approximations discussed in this article, the inversion for the weighting factors w_j of individual subfaults (point sources) in equation (4) can be made faster.

For the Sierra Madre earthquakes, we were not able to discern the fault plane from its conjugate plane. Our experiments indicate that the vertical component of the directivity, i.e., updip or downdip rupture, is not well constrained with regional records. This is partially due to the fact that regional rays usually have large take-off angles that make them less sensitive to vertical component of the rupture (e.g., S, S^{ss}, SdS, Fig. 4). The rays SmS and $sSmS$ would have the most power to resolve updip or downdip rupture, but the interplay between the down-going phases such as SmS and up-going phases such as direct S and S^s (Fig. 4) makes it more difficult to detect. Local data are more sensitive to the rupture direction for a given fault size, but adding just one local station (PAS) did not solve the problem. In the last experiment, the preferred rupture direction is westward and downdip on the fault plane or westward and updip on the conjugate plane. Note for a thrust or normal event, the fault plane and its conjugate plane have similar strike directions. When both planes have medium dip angles, which was the case for the 1991 Sierra Madre earthquake, this type of source mechanism is intrinsically more difficult, compared to other types of mechanisms, for any method using far-field data to distinguish rupture on fault plane or on its conjugate plane. With better station coverage and improved Green's functions, the situation should improve.

It is well known that the seismogram amplitude is a very important piece of information to use in the study of the source directivity (e.g., Kanamori *et al.*, 1992). As discussed earlier, the amplitude ratio between the data and synthetics varies significantly from station to station (Figs. 8 and 11). Rupture on finite faults predicts these ratios better than does the point source. However, any significant station bias on the seismic moment would obscure the picture. In a study of the Landers sequence, Jones (1995) reported that the long-

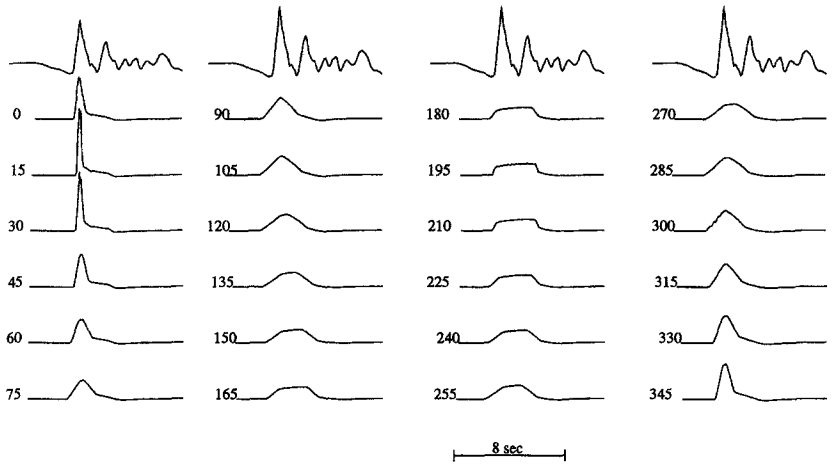

Figure 8. Comparison between data (PAS, tangential motion, the first trace in each column) and synthetics for fault size 5 × 5 km and varying rupture angles. Seismograms in each column are aligned in absolute timing and scaled with respect to peak amplitude. Numbers indicate rupture angles.

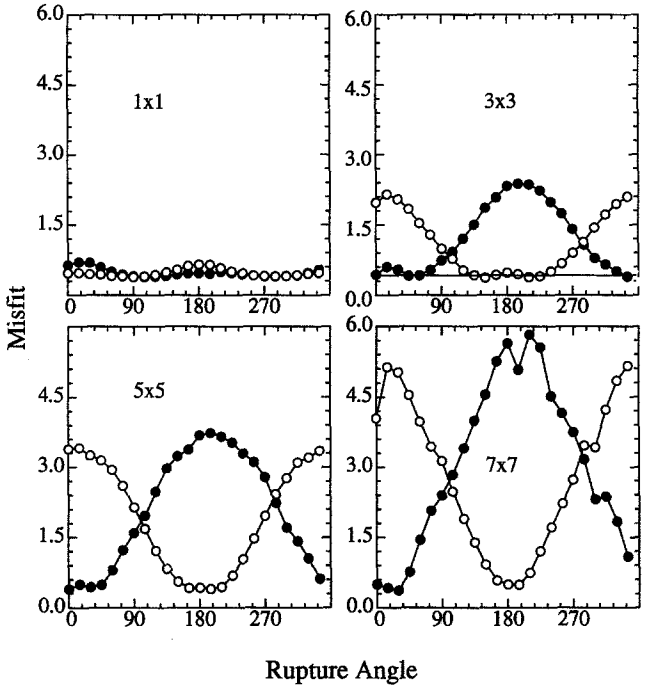

Figure 9. Misfit between data and synthetics as a function of rupture angle on the fault plane (solid circles) for different fault dimensions. Only the tangential motion at station PAS is used in this test. Open circles are for rupture on the conjugate plane. Rupture settings are the same as in Figure 5. Model LOHS1 (Table 1) is used. The straight line in the 3 × 3 box indicates the misfit value for synthetics with Dreger and Helmberger's (1991) point source.

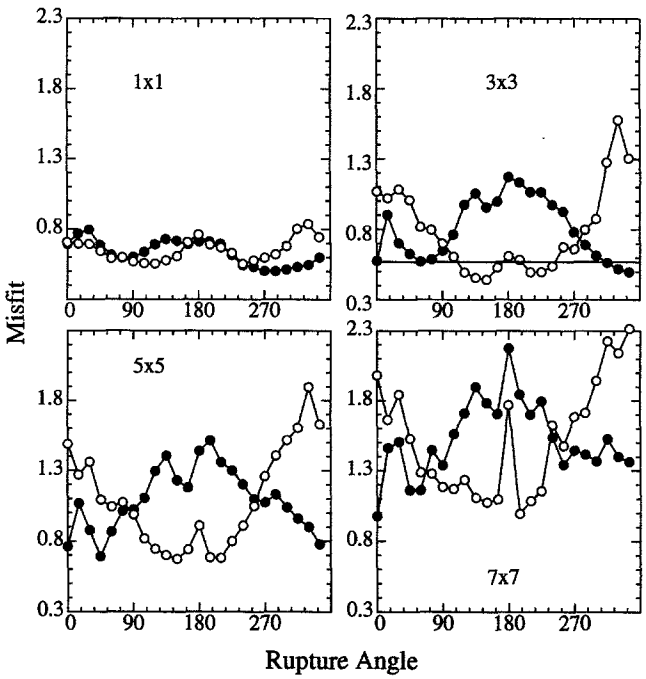

Figure 10. Misfit between data and synthetics as a function of rupture angle on the fault plane (solid circles) for different fault dimensions. Tangential displacement data at stations PAS, GSC, and PFO are used. Open circles are for rupture on the conjugate plane. Rupture settings are the same as in Figure 5. Model SC is used for stations GSC and PFO. Model LOHS1 is used for station PAS. The straight line in the 3 × 3 box indicates the misfit value for synthetics with Dreger and Helmberger's (1991) point source.

period seismic moment for station GSC is consistently greater (by 20%) than for PFO. Song *et al.* (1995) also noticed similar phenomena in their source study of the Northridge aftershocks. Thus, to reliably use the amplitude information in directivity studies, such station bias needs to be established. Fortunately, with the expanding broadband network, it will become possible to calibrate such effects for individual stations.

In summary, we developed a numerical method based on the generalized ray theory to efficiently calculate synthetic seismograms from complex finite-faulting processes. The approximations in this method are justified when the fault dimension is small compared to the source-receiver distance and when the structure around the source region is relatively simple so that the whole rupture region resides in

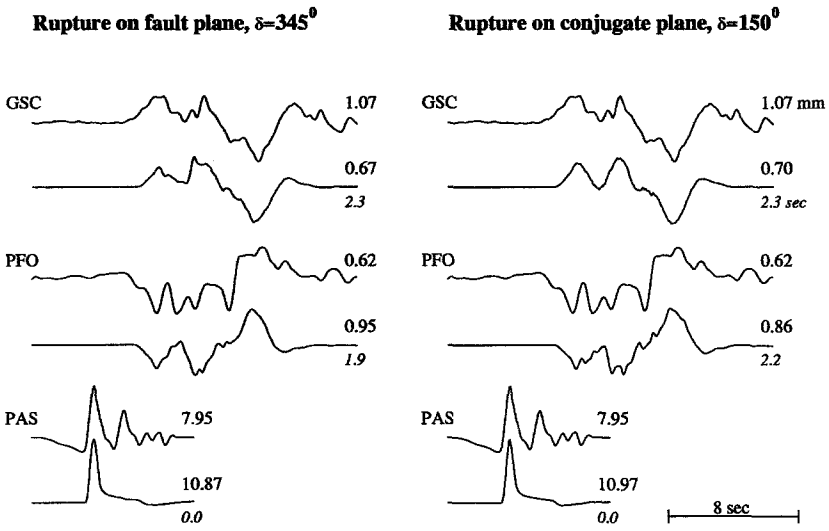

Figure 11. Comparison between data and synthetics for stations GSC, PFO, and PAS. The fault size is 3×3 km^2. A seismic moment of 3.1×10^{17} N·m is used for synthetics, as determined in the modeling process. Seismogram amplitudes are given in millimeters, and the time shift between data and synthetics are given in seconds.

a constant velocity layer. This method is applied in a grid-search approach to estimate the finite-source characteristics of the 1991 Sierra Madre earthquake with simple source models. Our results indicate westward rupture with a fault dimension of about 3 km, which are generally consistent with those of Wald (1992). Local data also proved usable and were particularly useful in our experiments.

Acknowledgments

We thank Craig Scrivner, Jennifer Scott, and Laura Jones for their reviews of the manuscript. Chuck Ammon and Jeroen Ritsema provided critical reviews along with very helpful suggestions. This research was supported by the Department of Defense and was monitored by the Air Force, Office of Scientific Research, under Contract F49620-93-1-0221, and by SCEC No. 645080 as funded by NSF 8920136. Contribution No. 5480, Division of Geological and Planetary Sciences, California Institute of Technology, Pasadena, California.

References

Dreger, D. and D. V. Helmberger (1991). Source parameters of the Sierra Madre earthquake from regional and local body waves, *Geophys. Res. Lett.* **18,** 11, 2015–2018.

Hartzell, S. H. and Thomas H. Heaton (1983). Inversion of strong ground motion and teleseismic waveform data for the fault rupture history of the 1979 Imperial Valley, California, earthquake, *Bull. Seism. Soc. Am.* **73,** no. 6, 1553–1583.

Haskell, N. A. (1964). Total energy and energy spectral density of elastic wave radiation from propagating faults, *Bull. Seism. Soc. Am.* **54,** no. 6, 1811–1841.

Helmberger, D. V. (1983). Theory and application of synthetic seismograms, in *Earthquakes: Observation, Theory and Interpretation,* Hiroo Kanamori (Editor), Soc. Italiana di Fisica, Bologna, Italy, 173–222.

Helmberger, D. V., D. Dreger, R. Stead, and H. Kanamori (1993). Impact of broadband seismology on the understanding of strong motions, *Bull. Seism. Soc. Am.* **83,** no. 3, 830–950.

Helmberger, D. V., R. Stead, Phyllis Ho-Liu, and D. Dreger (1992). Broadband modelling of regional seismograms: Imperial Valley to Pasadena, *Geophys. J. Int.* **110,** 42–54.

Jones, L. E. (1995). Broadband modeling of aftershocks from the Joshua Tree, Landers, and Big Bear sequences, southern California, *Ph.D Thesis,* California Institute of Technology, Pasadena, California.

Kanamori, H., H. Thio, D. Dreger, E. Hauksson, and T. Heaton (1992). Initial investigation of the Landers, California, earthquake of 28 June 1992 using TERRAscope, *Geophys. Res. Lett.* **19,** no. 22, 2267–2270.

Langston, C. (1978). The February 9, 1971 San Fernando earthquake: A study of source finiteness in teleseismic body waves, *Bull. Seism. Soc. Am.* **68,** no. 1, 1–29.

Patton, H. J. and G. Zandt (1991). Seismic moment tensors of western United States earthquakes and implications for the tectonic stress field, *J. Geophys. Res.* **96,** 18245–18259.

Ritsema, J. and T. Lay (1995). Long-period regional wave moment tensor inversion for earthquakes in the western United States, *J. Geophys. Res.* **100,** no. B7, 9853–9864.

Saikia, C. K. and D. V. Helmberger (1996). A frequency-wavenumber algorithm to compute up- and down-going wavefields from a buried seismic source, *Bull. Seism. Soc. Am.* **86,** 000–000.

Scrivner, C. W. and D. V. Helmberger (1995). Preliminary work on an early warning and rapid response program for moderate earthquakes, *Bull. Seism. Soc. Am.* **85,** no. 4, 1257–1265.

Song, X. J., C. W. Scrivner, and D. V. Helmberger (1995). Source characteristics of Northridge aftershocks, with application to the effect of San Fernando Basin on the propagation of seismic energy, *EOS* **76,** no. 46, F356.

Thio, H.-K. and H. Kanamori (1995). Moment tensor inversion for local earthquakes using surface waves recorded at TERRAscope, *Bull. Seism. Soc. Am.* **85,** no. 4, 1021–1038.

Wald, D. J. (1992). Strong motion and broadband teleseismic analysis of the 1991 Sierra Madre, California, earthquake, *J. Geophys. Res.* **97,** 11033–11046.

Walter, W. (1993). Source parameters of the June 29, 1992 Little Skull Mountain earthquake from complete regional waveforms at a single station, *Geophys. Res. Lett.* **20,** 403–406.

Zhao, L. and D. V. Helmberger (1994). Source estimation from broadband regional seismograms, *Bull. Seism. Soc. Am.* **84,** no. 1, 91–104.

Zhu, L. and D. V. Helmberger (1995). Advancement in source estimation techniques using broadband regional seismograms, EOS **76,** no. 46, F424.

Seismological Laboratory 252-21
Division of Geological and Planetary Sciences
California Institute of Technology
Pasadena, California 91125

Manuscript received 16 December 1994.